Image Processing and Classification Procedures for Analysis of Sub-decimeter Imagery Acquired with an Unmanned Aircraft over Arid Rangelands

Andrea S. Laliberte[1]
Jornada Experimental Range, New Mexico State University, Las Cruces, New Mexico 88003

Albert Rango
USDA-Agricultural Research Service, Jornada Experimental Range, Las Cruces, New Mexico 88003

Abstract: Unmanned aerial systems (UAS) have great potential as a platform for acquiring very high resolution aerial imagery for vegetation mapping. However, image processing and classification techniques require adaptation to images obtained with low-cost digital cameras. We developed and evaluated an image processing workflow that included the integration of resolution-appropriate field sampling, feature selection, and object-based image analysis for the purpose of classifying rangeland vegetation from a five-centimeter-resolution UAS image mosaic. Classification tree analysis was used to determine the optimal spectral, spatial, and contextual features. Segmentation and classification rule sets were developed on a test plot and were applied to the remaining study area, resulting in an overall classification accuracy of 78% at the species level and 81% at the structure-group level. The image processing approach provides a roadmap for deriving quality vegetation classification products from UAS imagery with very high spatial, but low spectral resolution.

INTRODUCTION

There is growing interest in using unmanned aerial systems (UAS) for remote sensing applications in natural resources. The increased use of UAS in military applications coupled with the miniaturization of flight computers, inertial sensors, and passive and active remote sensors (Patterson and Brescia, 2008) has led to greater application possibilities for UAS in the civilian sector. Large UAS have been used successfully for wildfire monitoring (Ambrosia et al., 2003) and for agricultural decision support (Herwitz et al., 2004; Johnson et al., 2004). Small UAS (<50 kg), however, offer several advantages for remote sensing applications. They have lower operating costs than large UAS, they can be deployed quickly and repeatedly, and because of low flying heights, they can acquire very high resolution imagery (Rango et al., 2009). Despite the potential as a platform for high-resolution vegetation monitoring, small

[1]Corresponding author; email: alaliber@nmsu.edu

GIScience & Remote Sensing, 2011, **48**, No. 1, p. 4–23. DOI: 10.2747/1548-1603.48.1.4

UAS have not found widespread use for this purpose. This can be attributed first to the difficulties in legally operating UAS in the National Airspace, and second, to the unique challenges associated with processing the imagery acquired with small UAS. The legalities of operating a UAS in the National Airspace have been described elsewhere (Dalamagkidis et al., 2008; Rango and Laliberte, 2010). In this paper, the focus is on the image processing aspects.

Due to low payload capabilities, small UAS are commonly equipped with lightweight, low-cost digital cameras, which can complicate the image processing workflow. In many cases, custom applications for photogrammetric processing and creation of orthomosaics are required to handle the large number of small-footprint images acquired with a rather unstable platform (Du et al., 2008; Laliberte et al., 2008; Wilkinson et al., 2009). In addition, while the images may have very high spatial resolution, the spectral and radiometric resolutions are often low, and image processing and classification procedures commonly used for satellite or aerial imagery require adaptation to this imagery.

For those reasons, some studies using imagery acquired with UAS have been based on the visual interpretation of soil or vegetation parameters, or the analysis of individual images (Hardin et al., 2007; Corbane et al., 2008; Hunt et al., 2010). Deriving vegetation maps from multiple UAS images combined into seamless image mosaics is less common. Dugdale (2007) used this approach to characterize intertidal flats, and Dunford et al. (2009) evaluated UAS image mosaics for mapping of Mediterranean riparian forests. Berni et al. (2009) obtained radiometrically corrected products for precision agriculture from UAS image mosaics, although they used a higher quality multispectral sensor.

Research into the use of small UAS for applied rangeland remote sensing has been ongoing at the USDA Agricultural Research Service's Jornada Experimental Range (Rango et al., 2009). Researchers have evaluated different UAS for rangeland mapping (Laliberte et al., 2007), assessed the regulations for operating UAS (Rango and Laliberte, 2010), and developed a workflow from image acquisition through classification (Laliberte et al., 2010). Throughout this work, the need to adapt the image processing and classification procedures to the UAS imagery has been recognized in three areas: (1) integration of resolution-appropriate field sampling; (2) determination of optimal features for analysis of this type of imagery; and (3) processing and analysis approaches suitable for UAS image mosaic files, which can be potentially large.

Regarding the first point, field samples obtained for training of classifiers and validation of classification maps have to be collected at a resolution appropriate to the image, because classification errors are directly affected by registration errors between imagery and field samples (Weber, 2006). GPS units are commonly used for collecting training and validation samples. A differentially corrected GPS unit can achieve submeter accuracy, but with 5 cm resolution UAS imagery, the GPS error still exceeds multiple pixels. A survey-grade GPS unit would be required to constrain the error to within a pixel. An additional source of error is the positional accuracy of the imagery, which is in the order of 1–2 m for image mosaics composed of 150–250 UAS images, covering 100–150 ha (Laliberte et al., in press).

The second area that required further investigation was the determination of optimal features for classification of this imagery. Spectral features are most useful for vegetation discrimination using multispectral satellite or aerial imagery, but the lack

of a near infrared band, and the high intercorrelation of the red (R), green (G), and blue (B) bands of low-cost digital cameras require evaluation of spatial, contextual, and texture features in addition to spectral features. Another option is the use of the intensity-hue-saturation (IHS) color space, in which intensity is separated from the dominant wavelength of color (hue), and saturation represents purity of color (Jensen, 2005). Conversion to IHS has proven useful for the analysis of RGB imagery from digital cameras for ground-based studies (Tang et al., 2000; Zheng et al., 2009), and for analysis of UAS imagery (Laliberte and Rango, 2008).

Feature selection methods range from graphical to statistical approaches (Jensen, 2005). For this study, we chose classification tree analysis (CTA; Breiman et al., 1998), because CTA is a nonparametric approach, and has been used successfully in conjunction with object-based image analysis (OBIA) in several studies (Chubey et al., 2006; Yu et al., 2006; Addink et al., 2010). The OBIA approach was chosen because of its suitability for very high resolution imagery, the ability to delineate ecologically meaningful image objects, and to derive spectral, spatial, and contextual features from these objects (Yu et al., 2006; Blaschke, 2010).

The third aspect of this study was to evaluate OBIA processing and analysis approaches suitable for large UAS image mosaic files. While the file size of a sub-decimeter image mosaic (e.g., 2 GB for a 180-image UAS mosaic) may not be large compared to traditional moderate-resolution satellite imagery, there are limits on the number of segments that can be created in the segmentation step of a fine-scale OBIA approach. Therefore, procedures for analyzing fine-resolution image mosaics in an object-based environment or for transferring the rule-base to larger areas are required. OBIA approaches for large areas have been addressed with QuickBird imagery (Johansen et al., 2010), but research into object-based classification of UAS image mosaics is in its infancy (Dunford et al., 2009; Laliberte et al., 2010).

Previous mapping efforts with these type of UAS image mosaics have focused mostly on broader vegetation classes at the structure-group level (i.e., grasses, shrubs, trees; Laliberte and Rango, 2008; Laliberte et al., 2010); therefore this study extends previous work by aiming at species-level vegetation mapping. The main purpose of this study was to evaluate an image processing workflow for species-level classification of sub-decimeter true-color digital camera imagery acquired with an UAS. Specifically, the following research questions were addressed: (1) Which field sampling procedure (GPS-based, on-screen digitizing, segment selection) is most appropriate for the image resolution? (2) What are the optimal features for an object-based species-level vegetation classification? (3) How well does the OBIA approach perform with respect to accuracy and transferability of the rule-base for relatively large UAS image mosaics?

METHODS

Study Area

The study area is located in southern New Mexico, in the southwestern corner of the Jornada Experimental Range (JER) (32°34′11″ N Lat., 106°49′44″ W Long.) (Fig. 1A), situated at the northern end of the Chihuahuan Desert. Mean annual precipitation is 245 mm, of which more than 50% occurs in July, August, and September

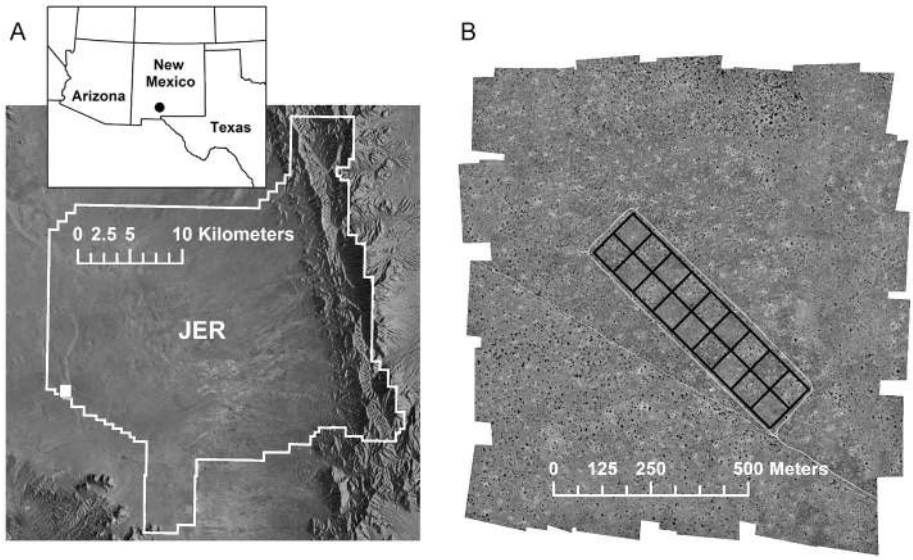

Fig. 1. Study area in southern New Mexico at the Jornada Experimental Range (JER) with UAS flight area delineated as a white polygon (A). UAS image mosaic over flight area with Stressor II study site outlined in black (B).

(Wainwright, 2006). The specific area of interest for this study was the Stressor II site (Fig. 1B), a nine ha area consisting of eighteen 0.5 ha plots established in 1996 to evaluate the effects of shrub removal and grazing treatments. The site was chosen because a vegetation classification was required for a related study. Dominant species at the site include honey mesquite (*Prosopis glandulosa* Torr.) (shrub), soap-tree yucca (*Yucca elata* Engleman.) (shrub-like), broom snakeweed (*Gutierrezia sarothrae* (Pursh) Britt. & Rusby) (sub-shrub), black grama (*Bouteloua eriopoda* Torrey) (grass), and dropseed (*Sporobolus* spp.) (grass). Litter was also prevalent, and was of interest in the mapping effort. The site represents a black grama–mesquite savanna on sandy soils (Fig. 2). Although the dominant shrub (mesquite) had previously been removed from several plots, all of the plots contain mesquite today to some extent due to shrub encroachment.

Unmanned Aircraft and Image Acquisition

The UAS used for image acquisition was a BAT 3 UAS, manufactured by MLB Co. (Mountain View, CA; Fig. 3). The BAT is a small UAS, with a gross weight of 10 kg, and a wingspan of 1.8 m. The UAS is fully autonomous and is launched by a catapult mounted on the top of a vehicle. A desired flight area was delineated with waypoints in the ground station software, and flight lines were generated automatically based on flying height to ensure image acquisition at 75% forward lap and 40% side lap for photogrammetric processing. The BAT carried two sensors: a video camera with live video downlink in the nose of the aircraft, and a Canon SD 900 10 megapixel digital camera mounted in the left wing. The images were stored on the camera's

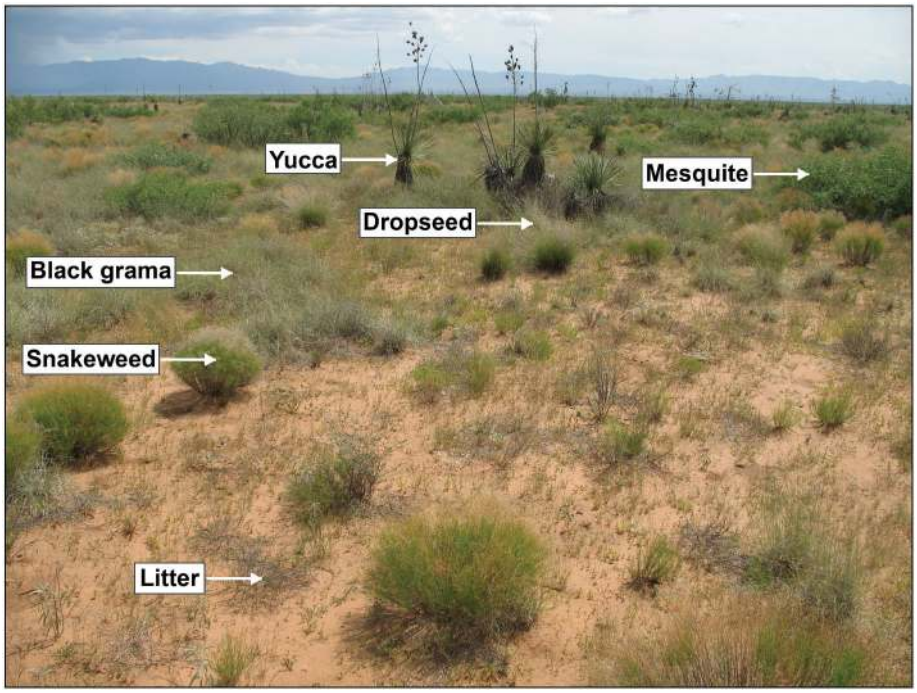

Fig. 2. Picture of study area with dominant species of interest for the mapping effort.

memory card, and the BAT's flight computer recorded a timestamp, GPS location, elevation, roll, pitch, and heading every time the camera's shutter was activated. The GPS had an update rate of four Hz, with an accuracy of 2.5 m. Roll, pitch, and heading were obtained with an inertial measurement unit (IMU), with an accuracy of ±2° for roll and pitch, and ±5° for heading. A data file containing location and attitude data was downloaded from the UAS after landing.

The imagery for this study was acquired on October 22, 2009 at a flying height of 210 m above ground with a ground resolved distance of 5 cm. An individual image footprint measured 213 m × 160 m at this flying height. To ensure sufficient coverage of the Stressor II site, we acquired 180 images in nine flight lines, and the total image collection area was approximately 130 ha.

Field Measurements

Field measurements comprised collection of (1) training and accuracy samples for one of the 0.5 ha plots, (2) accuracy samples for the entire study site, and (3) transect-based sampling to determine percent cover by species for the study site. Before collection of the actual training/accuracy samples, we conducted a sample collection test to determine which of the following three methods was most appropriate for the image resolution and the object-based image analysis at the species level: (1) GPS-based, (2) on-screen digitizing, and (3) segment selection. We considered this assessment an important step because it was a requirement that the field sample data had a tight

Fig. 3. BAT 3 UAS. The digital camera is mounted in the left wing, and the video camera is in the nose of the aircraft.

fit with the imagery for deriving appropriate features for subsequent classification. In addition to evaluating the accuracy of the GPS-based field samples, we also determined the efficiency of sample collection, because it was desirable to obtain a large sample size with a minimum time and effort.

All three methods were conducted in the field. The GPS-based method consisted of walking around patches of grass or shrub canopies with a Trimble® Pro XR differential GPS unit. For the on-screen digitizing method, we digitized vegetation patches directly on the UAS mosaic displayed in ArcPad® on a Tablet PC. In the segment selection method, the polygons derived from the segmentation step in the object-based analysis were displayed over the image and were selected on-screen. The on-screen digitizing and segment selection were done in the field while confirming the location of the vegetation patches on the high-resolution imagery displayed on the Tablet PC. For each method, 10 samples were collected, and all methods were evaluated in terms of efficiency and ease of use. For the GPS-based method, positional accuracy was also assessed by comparing the centroids of the GPS-based polygons with those of the on-screen–digitized polygons.

Results indicated that the best of the three methods was on-screen digitizing (see details in Results and Discussion section); this method was used to collect 677 samples for one of the plots. Half of the samples were used as training samples for feature selection and classifier training, and half were retained for accuracy assessment of the plot. For the accuracy assessment of the entire study site, we collected 771 samples with the same field method.

The purpose of the transect sampling was to compare image-based and ground-based estimates of percent cover. Transect sampling consisted of collecting line-point intercept data following a standard rangeland monitoring protocol (Herrick et al., 2005). In each of the 18 plots, seven transects were sampled at 10 cm intervals. At each interval, a pin was dropped to the ground, and plant species or soil surface condition (litter, bare ground) was recorded. Using only the first intercept of vegetation or soil to correspond with the image-based assessment, percent cover by species was calculated by dividing the number of hits for each species by the number of samples. Percent cover by species from ground measurements was compared with estimates derived from image classification for the study area.

Image Processing and Classification

The image processing workflow included orthorectification, mosaicking, image classification, and accuracy assessment. For UAS image processing, we have developed a custom, semi-automated approach (PreSync) that minimizes or eliminates the need for manual tie points and ground control points in the orthorectification process, and is suitable for processing hundreds of UAS images (Laliberte et al., 2008). PreSync was designed to improve the UAS's exterior orientation data (X, Y, Z, roll, pitch, heading), which has relatively low accuracy. After completion of PreSync, orthorectification and mosaicking of the imagery was performed using Leica Photogrammetry Suite (LPS®) (Erdas, 2010). Validations of mosaics created with this process have resulted in positional accuracies of approximately 1 m in flat terrain (Laliberte et al., in press), as in this study area. The image mosaic (Fig. 1B) was then subset to the Stressor II study site.

For the image analysis, we used eCognition® 8 (Definiens, 2009). The first step in the OBIA workflow was image segmentation, and at the fine scale required for the species-level classification, the study area could not be segmented in its entirety because of limitations on the number of image objects that could be generated in the software. Common workarounds for this limitation include: (1) a tiling and stitching approach, where the image can be subset into smaller tiles, which are segmented separately and subsequently stitched together (Johansen et al., 2010); or (2) tiling the image using a chessboard segmentation, followed by segmentation and classification of the chessboard tiles (Laliberte et al., 2010). The first workaround can only be applied in the server version of the software, while the second option can be used in the workstation version.

For the Stressor II study site, the second workaround approach was used. A vector file of the plot outlines constrained the chessboard segmentation, so that the tiles represented the 18 plots. We developed a rule set on one of the tiles (plots), and then applied it to the rest of the study area. The entire image analysis rule set, consisting of the tiling procedure, segmentation, class development, and classification rules, was compiled in a process tree.

The OBIA workflow and class hierarchy are shown in Figure 4. Plot 11 was chosen for development of the rule set because all vegetation classes (i.e. *Bare, Shadow, Large mesquite, Small mesquite, Snakeweed, Yucca, Black grama, Dropseed,* and *Litter*[2])

[2]Vegetation classes are indicated in italics in this paper.

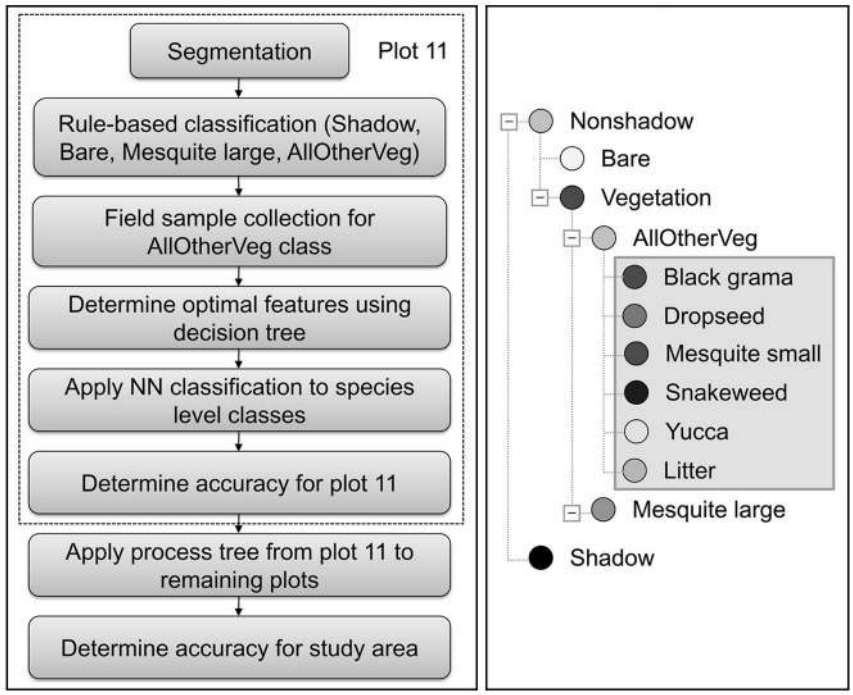

Fig. 4. Flowchart of object-based image analysis (left), and class hierarchy (right). In the class hierarchy, a nearest neighbor classification was applied to the classes in the grey box, while the remaining classes were classified using a rule-based classification.

were well represented. For the final classification, *Large mesquite* and *Small mesquite* were combined into a *Mesquite* class. Segmentation in eCognition® is controlled by a scale parameter, and a homogeneity criterion composed of color/shape and compactness/smoothness, both of which are weighted from 0 to 1 (Definiens, 2009). The image was segmented at two scales, a fine-scale segmentation (scale parameter 5, color/shape 0.9/0.1, compactness/smoothness 0.5/0.5), and a coarser scale spectral difference segmentation with a maximum spectral difference of 5. The spectral difference segmentation resulted in aggregation of adjacent segments of similar spectral response, while retaining spectrally unique segments within—i.e., small shrubs within a larger bare area were retained while the number of segments for the bare areas could be reduced. All classifications were executed at the spectral difference segmentation level.

We combined a rule-based and nearest neighbor classification with a masking procedure. The first step was a rule-based classification, separating the image first into *Shadow/Nonshadow*, and second *Nonshadow* into *Bare/Vegetation* using intensity. *Vegetation* was then classified into *Large mesquite/AllOtherVeg* by using an area greater than 1.6 m^2 to delineate *Large mesquite*. At this point, species-level field samples for plot 11 were collected in the area classified as *AllOtherVeg*. Those samples served as input for a decision tree or classification tree analysis (CTA) to determine the optimal spectral, spatial, and contextual features. Those features were used to further classify the *AllOtherVeg* class to the species level using a nearest neighbor classifier,

a classifier that searched for the closest sample image object in the feature space of each image object.

After an accuracy assessment of plot 11, the process tree was applied to the remaining plots. Finally, an accuracy assessment was conducted for the study area using 771 samples and determining overall, producer's, and user's accuracies, and Kappa indices (Congalton and Green, 2009) (Fig. 4).

Feature Selection

For the 339 training samples collected in plot 11, we extracted segment-based information for 22 features as a base for the feature selection process. The selection of the initial 22 features was based on previous analysis of UAS images acquired with a digital camera over similar vegetation communities. Spectral, spatial, and contextual features were included (Table 1). In addition to IHS, we used three vegetation indices that were modifications of the normalized difference vegetation index (NDVI) (Rouse et al., 1974). Because a near infrared band was not available, the modified NDVI was calculated using the red and green bands (Hunt et al., 2005), the red and blue bands, and the green and blue bands (NDVI RG, NDVI RB, NDVI GB). The spatial features (Area, Density, Roundness) were used to exploit the differences in size and shape of plants and patches.

The first feature selection step was to conduct Spearman's rank correlation analysis to eliminate features that had correlation coefficients (r_s) greater than 0.9. Sample information from the remaining uncorrelated features was used as input to the CTA, for which we used CART® (Salford Systems) (Steinberg and Colla, 1997). Algorithms in CART® are based on the work of Breiman et al. (1998). The optimum features were ranked based on the variable importance scores of the primary splitters in the tree. Scores had a range of 0–100 (100 = highest) and reflected the contribution of each feature in predicting the output classes.

RESULTS AND DISCUSSION

Field Sampling

The test of the three field sample collection methods (GPS-based, on-screen digitizing, segment selection) showed that the on-screen digitizing method was the most efficient and easy to use. Comparisons of the centroid coordinates of the GPS-based polygons with those of the on-screen digitized polygons showed an average difference and standard deviation of 0.97 ± 0.12 m ($n = 10$). A visual comparison of the polygons obtained with these two methods showed that with the exception of the larger shrubs, this error would make it difficult to determine which vegetation patch a GPS-based polygon belonged to. For that reason, the GPS-based method was deemed unsuitable.

We had hoped that the segment selection would be the preferred method, because this would have allowed us to directly import the segments as samples into eCognition®. However, some of the segments were too small to consistently allow for easy selection on the Tablet PC. The combination of bright sun and the use of a stylus to select some relatively small segments proved tedious. The on-screen digitizing method was the most rapid approach, as patches of interest could be delineated relatively quickly

Table 1. Features Used in the Object-Based Image Analysis, and Features Selected through Correlation Analysis and CTA Analysis[a]

Feature description	Input features[b] (22)	Uncorrelated features (16)	CTA-selected features (10)	Variable importance score
Mean band value	Mean R			
	Mean G	X		
	Mean B	X		
Mean band value divided by sum of band means	Ratio R	X	X	20.36
	Ratio G			
	Ratio B	X	X	52.40
NDVI for respective bands	NDVI RG	X	X	100.00
	NDVI RB			
	NDVI GB			
Standard deviation of band values	StdDev R	X		
	StdDev G	X	X	26.71
	StdDev B	X	X	37.74
Difference in mean band values between neighboring image objects	Mean diff. to neighbor R	X		
	Mean diff. to neighbor G	X		
	Mean diff. to neighbor B	X	X	44.28
(Max (R,G,B) – Min (R,G,B))/ brightness	Max. difference			
Mean hue	Hue	X	X	65.64
Mean intensity	Intensity	X		
Mean saturation	Saturation			
Area of image object	Area	X	X	74.93
Area of image object/ radius of image object	Density	X	X	18.84
Radius of smallest enclosing ellipse – radius of largest enclosed ellipse	Roundness	X	X	37.44

[a]Of the 22 input features, 16 uncorrelated features ($r_s < 0.9$) were used in the CTA, which selected 10 features. The variable importance scores are based on the primary splitters in the classification tree. The highest score is 100.
[b]R, G, B = red, green, and blue bands, respectively.

on-screen. It was not necessary to delineate the boundary of a patch in every detail in the field, because the file with the digitized patches was not imported directly into eCognition®. Instead, in the office we selected the sample segments manually based

on the on-screen digitized polygons displayed simultaneously in ArcPad®. This approach avoided potential misalignments between imported digitized polygons and the segment outlines.

With coarser resolution imagery the effect of the GPS error would be reduced. For example, using 4 m multispectral IKONOS satellite imagery, Karl and Maurer (2009) were able to determine the location of sample sites to within 1 pixel. Our fine-scale mapping requirements coupled with GPS error and positional accuracies of the orthomosaics made the use of GPS for delineating polygons problematic on the fine-scale UAS imagery. On-screen digitizing ensured that the correct sample was selected on the image. In addition to on-screen digitizing, we also found that a printed output of the image was helpful for general navigation and adding additional notes to the print-out. With a survey-grade GPS, the positional error could be reduced considerably, and the GPS data could be imported directly into eCognition® as sample objects.

Feature Selection

Of the 22 input features, 16 were uncorrelated ($r_s > 0.9$). Out of those 16, CART® selected 10 features. Six were spectral features (Ratio R, Ratio B, NDVI RG, StdDev G, StdDev B, Hue), three were spatial features (Area, Density, Roundness), and one was a contextual feature (Mean difference to neighbor B). The four highest variable importance scores were assigned to NDVI RG, Area, Hue, and Ratio B (Table 1). The results demonstrate the necessity of incorporating spectral, spatial, and contextual features for the classification of this type of imagery, and the advantage of using a feature selection approach such as CTA. It is not always easy to predict which features or feature combinations will work best. In this study area, we expected selection of the other two shape features, Density and Roundness, because snakeweed is characteristically round. Intensity was also not included, but has been proven useful in previous UAS image classifications (Laliberte and Rango, 2008). Intensity was the most suitable feature for the first-step rule-based classification for separating *Bare* and *Vegetation* in this study, although the selection was based on visual assessment using the feature view tool in eCognition®.

Texture features were not used in this study for two reasons. First, we assumed that the fine-scale segments would not be conducive to texture analysis. Second, previous studies indicated that although texture could increase classification accuracies with this imagery, the inclusion of IHS resulted in comparable accuracies and required considerably less computation time (Laliberte and Rango, 2008). Texture measures are time consuming to compute, and with multiple images to process, computation time had to be considered.

Classification Workflow

The workflow of developing the rule set on one plot (tile), and applying it to the other 17 tiles was efficient and consistent. Initial development of the rule set on plot 11 took approximately six hours. Segmenting and classifying the entire study area required 1.5 hours. No editing was done, because we wanted to assess the transferability of the rule set by evaluating the classification accuracy.

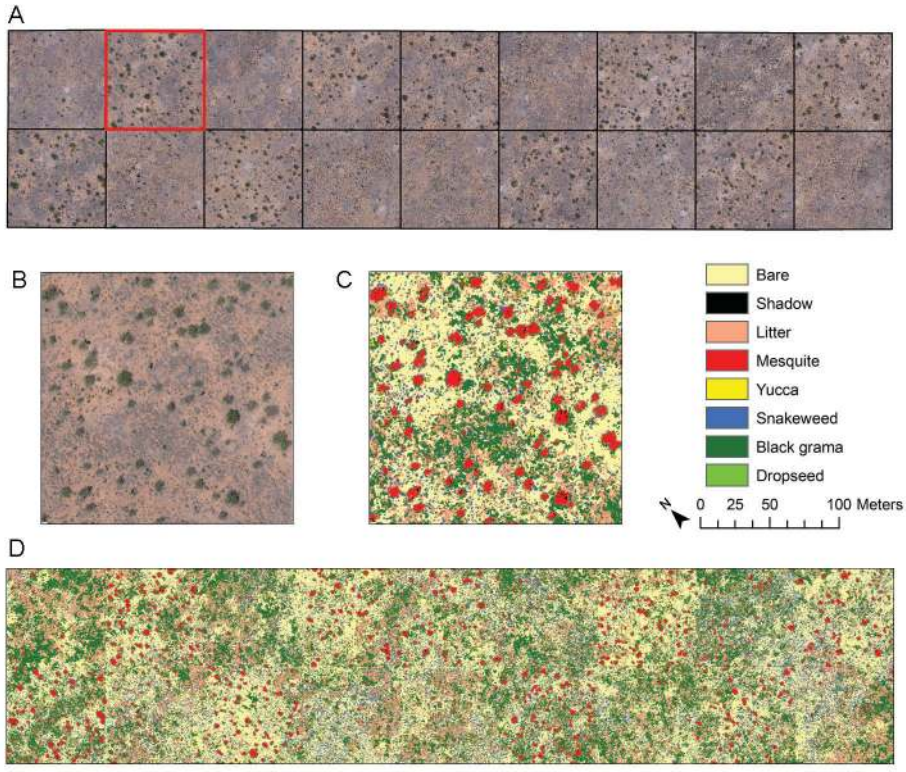

Fig. 5. Stressor II study site and classification. UAS image mosaic of study site with grid of 18 plots overlaid (A). Outlined in red in (A) is the 0.5 ha plot (B), where the rule set for the classification (C) was developed, and then applied to the entire study site (D). The scale bar applies to (A) and (D).

The image of the Stressor II study site shows the variability in mesquite cover due to shrub removal in some of the plots (Fig. 5A). The rule set was developed in plot 11 (Fig. 5B, classification in Fig. 5C). The classification of the entire study site (Fig. 5D) demonstrates the transferability of the rule set, visually most noticeable here for *Mesquite*, which is most discernable in the figure. Choosing separate classes for *Large mesquite* and *Small mesquite* proved advantageous. *Large mesquite* was defined by rules including a spectral (Intensity) and a spatial (Area) feature, which made this class unique, reduced confusion with similar spectral objects, and increased accuracy for the *Mesquite* class. Even though some plots had relatively few *Large mesquite*, the rules from plot 11 had equally good results in all plots. An attempt to define a large shrub strictly with spectral features would likely be less transferable with this type of imagery. On the other hand, using such specific rules was not possible with the other six species-level classes (including *Small mesquite*), because visual interpretation alone could not detect unique spectral or spatial features for those classes. Therefore, a nearest neighbor classifier was more suitable to define those classes.

The object-based hierarchical classification approach incorporating masking techniques proved to be well suited for transfer to other image tiles. Although the

Table 2. Error Matrix for Classification of Plot 11[a]

	Bare	Litter	Mesquite	Yucca	Snake-weed	Black grama	Dropseed
Bare	79,815	26,450			100		
Litter	21,717	440,462			116	1,367	
Mesquite	123	254	104,759	13,639	9,477	1,548	62
Yucca	81	447	832	13,365	7,124	1,948	81
Snakeweed	65	208		766	14,859	2,122	
Black grama		110,200	370		112	50,624	116
Dropseed		1,521	65		705	2,876	1,687
Producer's accuracy, pct.	78	76	98	48	46	84	87
User's accuracy, pct.	75	95	81	56	82	31	25
Overall accuracy, pct.	78						
Kappa index	0.64						

[a]Classification data are in rows, reference data in columns. Values for classes are pixels.

thresholds for the rule-based classes (*Shadow/Nonshadow, Bare/Vegetation, Large mesquite/AllOtherVeg*) were not edited because the study area was relatively homogenous, such edits could be applied to individual tiles if necessary. The transferability of rule sets is a relatively new research topic in OBIA, and has mostly been explored with high-resolution satellite imagery in urban areas (Schöpfer and Möller, 2006; Walker and Blaschke, 2008). Using this approach with UAS imagery can potentially provide a tool for rangeland monitoring over even larger areas due to the efficiency of a remote sensing approach over ground-based measurements (Laliberte et al., 2010). Using the server version of eCognition, the methods described here could be applied in a tiling and stitching approach, which would allow for processing even larger images in an efficient manner, as long as the vegetation in the larger image was similar to the area where the training samples were collected.

Classification Accuracy

The classification accuracy was assessed at two steps of the image analysis process: for the classification of plot 11, and for the entire Stressor II study site. The overall accuracy for plot 11 was 86% with a Kappa index of 0.81 (Table 2). *Bare* had the highest user's and producer's accuracies, followed by *Mesquite* and *Black grama*, and *Litter* had the lowest accuracies due to confusion with the spectrally similar *Black grama*. *Mesquite* and *Yucca* were also confused with each other. The error matrix for the classification of the study area showed an overall accuracy of 78%, with a Kappa index of 0.64 (Table 3). Compared to the plot 11 error matrix, both user's and producer's

Table 3. Error Matrix for Classification of Stressor II Study Area at the Species Level[a]

	Bare	Litter	Mesquite	Yucca	Snake-weed	Black grama	Dropseed
Bare	7,385	28		2		5	1
Litter		1,750	79	9	279	1,334	32
Mesquite		46	9,853			1	
Yucca		3	522	492	14	21	2
Snakeweed		67	18		698	72	
Black grama		1,357	22	70	288	5,998	22
Dropseed					18		35
Producer's accuracy, pct.	100	54	94	86	54	81	38
User's accuracy, pct.	99	50	99	46	81	77	66
Overall accuracy, pct.	86						
Kappa index	0.81						

[a]Classification data are in rows, reference data in columns. Values for classes are pixels.

accuracies were lower for *Bare*, and higher for *Litter*, and approximately the same for *Mesquite* and *Snakeweed. Black grama* and *Dropseed* had lower user's accuracies.

At the plot level, very few classes were confused with *Bare*, while at the study area-level, *Bare* and *Litter* were confused to a greater extent. This was attributed to the transfer of the rule set. The Intensity threshold for *Bare* in plot 11 (as for all thresholds) was chosen specifically for that plot, and some variation in that threshold had to be expected for other plots. There was also confusion between *Black grama* and *Litter*, and *Black grama* and *Dropseed.* Table 3 shows that for the reference samples, the area not assigned to *Black grama* was mostly *Dropseed*, although *Snakeweed, Yucca, Mesquite*, and *Litter* were also confused with *Black grama*. *Dropseed* proved to be a challenge to map. Its small size and extent in the study area probably contributed to the low user's accuracy.

The transfer of the classification routine had mixed results with regard to accuracies in species-level classes. While larger (*Mesquite*) or distinctly shaped (*Snakeweed*) shrubs had comparable accuracies at the plot and the study area scale, smaller and/or less spectrally distinct grasses had lower user's accuracies. The lower accuracies in *Bare* for the study area compared to the plot can be attributed to the confusion with *Litter*. *Bare* is usually one of the easiest classes to distinguish with this imagery, and has resulted in higher user's and producer's accuracies in other mapping efforts (Laliberte et al., in press). While the accuracies for *Litter* in the study area were relatively good, we believe that attempting to map litter contributed to lower accuracies in the *Bare* and *Black grama* classes. *Litter* was also a highly variable class, because

Table 4. Error Matrix for Classification of Stressor II Study Area at the Structure-Group Level[a]

	Bare	Litter	Shrubs	Grasses
Bare	79,815	26,450	100	
Litter	21,717	440,462	116	1,367
Shrubs	270	909	164,822	5,761
Grasses		111,721	1,251	55,302
Producer's accuracy, pct.	78	76	99	88
User's accuracy, pct.	75	95	95	33
Overall accuracy, pct.	81			
Kappa index	0.70			

[a]Classification data are in rows, reference data in columns. Values for classes are pixels.

it was confused with *Bare* when the density of litter was low, and with *Black grama* at higher litter densities.

In 2008, the same type of UAS imagery was acquired over an Idaho sagebrush community for mapping vegetation at the structure-group level for a 116 ha site, and at the species level for six 0.25 ha plots (Laliberte et al., 2010). Results from the Idaho study provide a useful point of reference for the Stressor II study site results. Classification accuracies obtained using a transferred rule-base were in the 80–90% range, and never lower than 60% for structure-group mapping in the Idaho study. In order to assess accuracies at the structure-group level for the Stressor II study site, we aggregated the error matrix into four classes, retaining *Bare* and *Litter*, and combining the rest into *Shrub* and *Grass*. The overall accuracy increased to 81%, with accuracies for *Shrub* in the high 90 percent range, and *Grass* at 88% producer's and 33% user's accuracy (Table 4).

Results of the Idaho study showed that differentiation into shrub species was possible if the percent cover values derived from line point intercept measures exceeded two percent cover in the image (Laliberte et al., 2010). The percent cover values obtained from ground based measurements at the Stressor II study site indicate that *Dropseed* (2.1%) and *Yucca* (1.3%) were near that limit (Fig. 6), indicating a similar threshold for species differentiation as in the Idaho study. The graph (Fig. 6) also shows relatively large differences between image- and ground-based estimates of percent cover for *Bare* and *Litter*, confirming the confusion of *Litter* with *Bare* and *Black grama*. Aggregating the percent cover data to the structure-group level resulted in smaller differences between image- and ground-based estimates of cover for the aggregated classes *Shrub* and *Grass* (Fig. 7). If *Bare* and *Litter* were to be combined into a non-vegetated class, the percent cover differences between image- and ground-based estimates would be reduced (58.9% image, 62.5% ground). For this particular vegetation community, we consider species mapping possible for *Mesquite*, and very likely for *Snakeweed* and *Black grama* if the highly variable class *Litter* is not included.

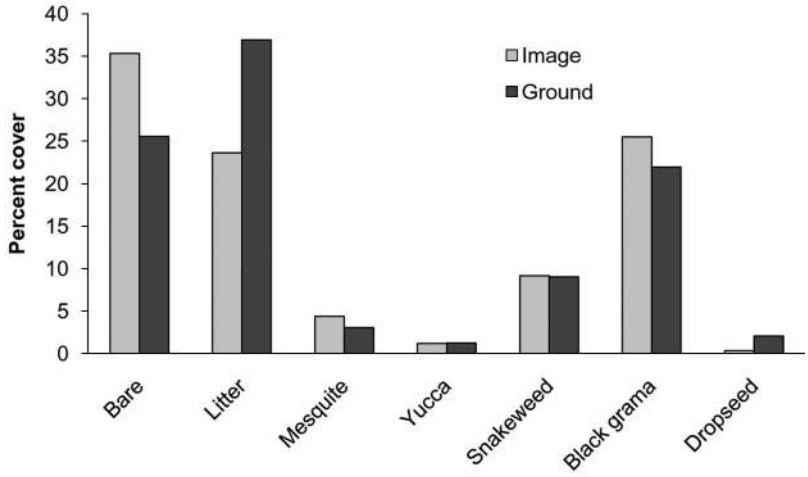

Fig. 6. Percent cover values for the Stressor II study site obtained from image classification and ground measurements at the species level.

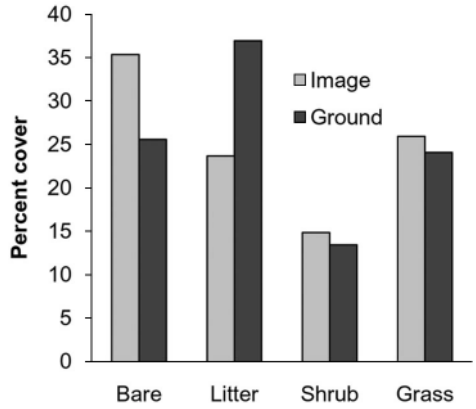

Fig. 7. Percent cover values for the Stressor II study site obtained from image classification and ground measurements at the structure-group level.

CONCLUSIONS

This study has evaluated an image processing workflow for detailed classification of sub-decimeter UAS image mosaics. Based on this and other studies using the same type of UAS imagery in arid rangelands, we conclude that mapping at the structure-group level is probably more appropriate and more repeatable than mapping at the species level using a transferred rule set. The error matrices and estimates of percent cover demonstrate the limit of separability between certain species-level classes that can be obtained with this imagery. This does not mean that species mapping cannot be achieved with this imagery, but rather that it depends on a species' spectral, spatial,

and contextual properties. These properties have to be assessed for each site and considered before defining the classes and the classification routine.

There are very few published studies on vegetation classifications of UAS-derived image mosaics. The creation of image mosaics can be a major hurdle for using UAS for monitoring purposes (Dugdale, 2007), although our process allows us to create image mosaics within days of flying. Dunford et al. (2009) evaluated 6–25 cm UAS imagery for mapping of Mediterranean riparian forests, and achieved overall classification accuracies of 63% and 71% (Kappa index 0.47 and 0.6, respectively) for four species-level classes, although they reported a decrease in accuracy for mosaic-level classifications compared to single image classifications. Wundram and Löffler (2008) used kite aerial photography to obtain 10 cm resolution digital camera imagery and mapped mountain vegetation in five classes with Kappa indices of 0.51 and 0.65, although only two images were used and classified. Given that we used a multi-image mosaic and a transferred rule-base for classification, our accuracy results compare favorably with the above studies.

The results of this study demonstrate that UAS-acquired very high resolution imagery provides detailed information for mapping and monitoring rangelands, which are a major portion of the world's land area. UAS are highly suited for flying remote sensing missions in those vast and remote areas due to the relatively low image acquisition costs and high flexibility. The integration of resolution-appropriate field sampling, feature selection, OBIA, and suitable processing approaches for UAS image mosaics provides a roadmap for deriving quality classification products from UAS imagery. The demonstrated approach is computationally efficient and scalable for classification of even larger areas of similar vegetation. The integration of spectral, spatial, and contextual features in an OBIA workflow can overcome to some degree the shortcomings of low-cost digital cameras used on many small UAS. As in any other classification project, the level of detail is highly dependent on the spectral and spatial uniqueness of the classes, and the analyst has to recognize the limitations of the sensor. Ongoing research is focused on further automation of the object-based image analysis approach, on testing the approach on larger areas, and on integration of other sensors into the UAS to take advantage of near infrared wavelengths for better vegetation discrimination.

ACKNOWLEDGMENTS

This research was funded by the USDA Agricultural Research Service and the National Science Foundation Long-Term Ecological Research Program, Jornada Basin IV: Linkages in Semiarid Landscapes. We would like to acknowledge the assistance of Peg Gronemeyer and Lauren Svejcar for field data collection efforts.

REFERENCES

Addink, E. A., de Jong, S. M., Davis, S. A., Dubyanskiy, V., Burdelow, L. A., and H. Leirs, 2010, "The Use of High-Resolution Remote Sensing for Plague Surveillance in Kazakhstan," *Remote Sensing of Environment*, 114:674–681.

Ambrosia, V. G., Wegener, S. S., Sullivan, D. V., Buechel, S. W., Dunagan, S. E., Brass, J. A., Stoneburner, J., and S. M. Schoenung, 2003, "Demonstrating UAV-Acquired

Real-Time Thermal Data over Fires," *Photogrammetric Engineering and Remote Sensing*, 69(4):391–402.

Berni, J. A. J., Zarco-Tejada, P. J., Suarez, L., and E. Fereres, 2009, "Thermal and Narrowband Multispectral Remote Sensing for Vegetation Monitoring from an Unmanned Aerial Vehicle," *IEEE Transactions on Geoscience and Remote Sensing*, 47(3):722–738.

Blaschke, T., 2010, "ObjectBased Image Analysis for Remote Sensing," *ISPRS Journal of Photogrammetry and Remote Sensing*, 65:2–16.

Breiman, L., Friedman, J. H., Olshen, R. A., and C. J. Stone, 1998, *Classification and Regression Trees*, Boca Raton, FL: CRC Press, 358 p.

Chubey, M. S., Franklin, S. E., and M. A. Wulder, 2006, "Object-Based Analysis of Ikonos-2 Imagery for Extraction of Forest Inventory Parameters," *Photogrammetric Engineering and Remote Sensing*, 72(4):383–394.

Congalton, R. G. and K. Green, 2009, *Assessing the Accuracy of Remotely Sensed Data: Principles and Practices*, Boca Raton, FL: CRC Press, 183 p.

Corbane, C., Raclot, D., Jacob, F., Albergel, J., and P. Andrieux, 2008, "Remote Sensing of Soil Characteristics from a Multiscale Classification Approach," *Catena*, 75:308–318.

Dalamagkidis, K., Valavanis, K. P., and L. A. Piegl, 2008, *On Integrating Unmanned Aircraft Systems into the National Airspace System*, New York, NY: Springer, 199 p.

Definiens, 2009, *eCognition Developer 8.0 User Guide*, Munich, Germany: Definiens AG.

Du, Q., Raksuntorn, N., Orduyilmaz, A., and L. M. Bruce, 2008, "Automatic Registration and Mosaicking for Airborne Multispectral Image Sequences," *Photogrammetric Engineering and Remote Sensing*, 74(2):169–181.

Dugdale, S., 2007, An Evaluation of Imagery from an Unmanned Aerial Vehicle (UAV) for the Mapping of Intertidal Macroalgae on Seal Sands, Tees Estuary, UK, M.Sc. thesis, Department of Geography, University of Durham.

Dunford, R., Michel, K., Gagnage, M., Piegay, H., and M.-L. Tremelo, 2009, "Potential and Constraints of Unmanned Aerial Vehicle Technology for the Characterization of Mediterranean Riparian Forest," *International Journal of Remote Sensing*, 30(19):4915–4935.

Erdas, 2010, *Erdas 2010 Field Guide*, Norcross, GA: Erdas, Inc.

Hardin, P. J., Jackson, M. W., Anderson, V. J., and R. Johnson, 2007, "Detecting Squarrose Knapweed (*Centaurea virgata* Lam. Ssp. *squarrosa* Gugl.) Using a Remotely Piloted Vehicle: A Utah Case Study," *GIScience and Remote Sensing*, 44(3):1548–1603.

Herrick, J. E., Van Zee, J. W., Havstad, K. M., Burkett, L. M., and W. G. Whitford, 2005, *Monitoring Manual for Grassland, Shrubland and Savanna Ecosystems. Volume I: Quick Start, and Volume II: Design, Supplementary Methods and Interpretation,* Las Cruces, NM: USDA-ARS Jornada Experimental Range.

Herwitz, S. R., Johnson, L. F., Dunagan, S. E., Higgins, R. G., Sullivan, D. V., Zheng, J., Lobitz, B. M., Leung, J. G., Gallmayer, B. A., Aoyagi, M., Slye, R. E., and J. A. Brass, 2004, "Imaging from an Unmanned Aerial Vehicle: Agricultural Surveillance and Decision Support," *Computers and Electronics in Agriculture*, 44:49–61.

Hunt, E. R., Cavigelli, M., Daugherty, C. S. T., McMurtrey, J., and C. L. Walthall, 2005, "Evaluation of Digital Photography from Model Aircraft for Remote Sensing of Crop Biomass and Nitrogen Status," *Precision Agriculture*, 6:359–378.

Hunt, E. R., Hively, W. D., Fujikawa, S. J., Linden, D. S., Daughtry, C. S. T., and G. W. McCarty, 2010, "Acquisition of NIR-Green-Blue Digital Photographs from Unmanned Aircraft for Crop Monitoring," *Remote Sensing*, 2:290–305.

Jensen, J. R., 2005, *Introductory Digital Image Processing: A Remote Sensing Perspective*, Upper Saddle River, NJ: Prentice Hall, Inc.

Johansen, K., Arroyo, L. A., Phinn, S., and C. Witte, 2010, "Comparison of Geo-object Based and Pixel-Based Change Detection of Riparian Environments Using High Spatial Resolution Multi-spectral Imagery," *Photogrammetric Engineering and Remote Sensing*, 76(2):123–136.

Johnson, L. F., Herwitz, S. R., Lobitz, B. M., and S. E. Dunagan, 2004, "Feasibility of Monitoring Coffee Field Ripeness with Airborne Multispectral Imagery," *Applied Engineering in Agriculture*, 20(6):845–849.

Karl, J. W. and B. A. Maurer, 2009, "Multivariate Correlations between Imagery and Field Measurements across Scales: Comparing Pixel Aggregation and Image Segmentation," *Landscape Ecology,* 25(4):591–605.

Laliberte, A. S., Herrick, J. E., Rango, A., and C. Winters, 2010, "Acquisition, Orthorectification, and Object-Based Classification of Unmanned Aerial Vehicle (UAV) Imagery for Rangeland Monitoring," *Photogrammetric Engineering and Remote Sensing*, 76(6):661–672.

Laliberte, A. S. and A. Rango, 2008, "Incorporation of Texture, Intensity, Hue, and Saturation for Rangeland Monitoring with Unmanned Aircraft Imagery," in *The International Archives of the Photogrammetry, Remote Sensing, and Spatial Information Sciences*, GEOBIA 2008, Calgary, Alberta, Canada, 5–8 Aug., ISPRS Vol. No. XXXVIII-4/C1, 6 p.

Laliberte, A. S., Rango, A., and J. E. Herrick, 2007, "Unmanned Aerial Vehicles for Rangeland Mapping and Monitoring: A Comparison of Two Systems," in *ASPRS Annual Conference Proceedings*, Tampa, FL, 7–11 May.

Laliberte, A. S., Winters, C., and A. Rango, 2008, "A Procedure for Orthorectification of Sub-decimeter Resolution Imagery Obtained with an Unmanned Aerial Vehicle (UAV)," in *ASPRS Annual Conference Proceedings*, Portland, OR, 28 April–2 May.

Laliberte, A. S., Winters, C., and A. Rango, in press, "UAS Remote Sensing Missions for Rangeland Applications," *Geocarto International*.

Patterson, M. C. L. and A. Brescia, 2008, "Integrated Sensor Systems for UAS," in *Proceedings of the 23rd Bristol International Unmanned Air Vehicle Systems (UAVS) Conference*, Bristol, UK, 7–9 April.

Rango, A. and A. S. Laliberte, 2010, "Impact of Flight Regulations on Effective Use of Unmanned Aircraft Systems for Natural Resources Applications," *Journal of Applied Remote Sensing*, 4:043539.

Rango, A., Laliberte, A. S., Herrick, J. E., Winters, C., Havstad, K. M., Steele, C., and D. M. Browning, 2009, "Unmanned Aerial Vehicle–based Remote Sensing for Rangeland Assessment, Monitoring, and Management," *Journal of Applied Remote Sensing*, 3:033542.

Rouse, J. W., Haas, R. J., Schell, J. A., and D. W. Deering, 1974, "Monitoring Vegetation Systems in the Great Plains with ERTS," in *Third Earth Resource Technology Satellite (ERTS) Symposium*, Washington, DC, 309–317.

Schöpfer, E. and M. S. Möller, 2006, "Comparing Metropolitan Areas—Transferable Object–Based Image Analysis Approach," *Photogrammetrie, Fernerkundung, Geoinformation*, 10(4):277–286.

Steinberg, D. and P. Colla, 1997, *CART—Classification and Regression Trees*, San Diego, CA: Salford Systems.

Tang, L., Tian, L., and B. L. Steward, 2000, "Color Image Segmentation with Genetic Algorithm for In-Field Weed Sensing," *Transactions of the American Society of Agricultural Engineers*, 43(4):1019–1027.

Walker, J. S. and T. Blaschke, 2008, "Object-Based Landcover Classification for the Phoenix Metropolitan Area: Optimization vs. Transportability," *International Journal of Remote Sensing*, 29(7):2021–2040.

Wainwright, J., 2006, "Climate and Climatological Variations in the Jornada Basin," in *Structure and Function of a Chihuahuan Desert Ecosystem. The Jornada Basin Long-Term Ecological Research Site,* Havstad, K. M., Huennecke, L. F., and W. H. Schlesinger (Eds.), Oxford, UK: Oxford University Press, 44–80.

Weber, K. T., 2006, "Challenges of Integrating Geospatial Technologies into Rangeland Research and Management," *Rangeland Ecology and Management*, 59:38–43.

Wilkinson, B. E., Dewitt, B. A., Watts, A. C., Mohamed, A. H., and M. A. Burgess, 2009, "A New Approach for Pass-Point Generation from Aerial Video Imagery," *Photogrammetric Engineering and Remote Sensing*, 75(12):1415–1423.

Wundram, D. and J. Löffler, 2008, "High-Resolution Spatial Analysis of Mountain Landscapes Using a Low-Altitude Remote Sensing Approach," *International Journal of Remote Sensing,* 29(4):961–74.

Yu, Q., Gong, P., Clinton, N., Biging, G., Kelly, M., and D. Schirokauer, 2006, "Object-Based Detailed Vegetation Classification with Airborne High Spatial Resolution Remote Sensing Imagery," *Photogrammetric Engineering and Remote Sensing*, 72(7):799–811.

Zheng, L., Zhang, J., and Q. Wang, 2009, "Mean-Shift-Based Color Segmentation of Images Containing Green Vegetation," *Computers and Electronics in Agriculture*, 65:93–98.